A potenciometriás pásztázó elektrokémiai mikroszkópia legújabb eredményei

Tézisfüzet

Szerző:
KISS ANDRÁS
Kémia Doktori Iskola
Általános és Fizikai Kémia Tanszék

Témavezető:
Prof. Dr. NAGY GÉZA
Általános és Fizikai Kémia Tanszék

Doktori Iskola vezetője:
Prof. Dr. KILÁR FERENC

Pécsi Tudományegyetem

2017. április 16.

1. Bevezetés

A Pásztázó Alagúthatás Mikroszkópia (STM, Scanning Tunnelling Microscopy) 1981-es feltalálása óta a felületanalízis hatalmas fejlődésnek indult. A módszer fontosságát jelzi, hogy megalkotójuk, Binni és Rohrer mindössze öt évvel később, 1986-ban Bonel-díjban részesültek úttörő munkájukért. Ez a technika volt az első Pásztázó Mérőcsúcs Mikroszkópiás (SPM, Scanning Probe Microscopy) technika, melyet sok hasonló követett. Közös bennük az a helyi mérés, melyet egy raszter minden egyes előre meghatározott pontján végzünk el. A mért paraméter helykoordináták mentén való ábrázolásával rajzolható meg a mikroszkópiás kép. Legfőbb előnyük a hagyományos optikai mikroszkópiához képest az elképesztő felbontásuk. Mivel a technikát nem korlátozza az Abbes képlet, egyedi atomok is „láthatóvá" tehetőek. Az eredeti STM technika változatai sorra jelentek meg az elkövetkező években. Az Atomerő Mikroszkópiát például 1982-ben találta fel, ugyancsak Binnig és Rohrer.

1989-ben alkották meg elektrokémikusok a módszer elektrokémiai változatát, a Pásztázó Elektrokémiai Mikroszkópiát (PEKM, SECM = Scanning Electrochemical Microscopy). A működési elv ugyanaz, a különbség csak a mérőcsúcsban rejlik. Ebben az esetben ez egy mikroelektród. A technikával kémiai információ térképezhető nagy felbontással, felületek egész soráról. Legnagyobb hátránya a viszonylag kis sebessége, mely a pásztázási folyamat következménye. Az egész képet ugyanazzal a mérőcsúccsal kell végigpásztázni, szemben például az optikai mikroszkópiával, ahol leggyakrabban egy szenzor mátrixot alkalmazunk képalkotási célra. Ennek az a következménye, hogy minél több pontól áll a kép, annál tovább tart a képalkotás. Ez különösen nagy probléma a PEKM potenciometriás üzemmódjában. A potenciometriás cella válaszidejét az időállandó írja le, mely főleg az indikátor elektród ellenállásától függ. A mikroelektródok kis méretükből adódóan rendkívül nagy ellenállásúak lehetnek, elérve akár a GΩ-os tartományt is. Ezért a képalkotás ideje jelentősen megnyúlhat, és általában percekben vagy akár órákban mérhető.

A többi pásztázó technika jelentősen gyorsult az utóbbi néhány évtizedben, és sebességük lehetővé teszi videók rögzítését is. Az alacsony sebesség azonban egy sokszor elhanyagolt korlátja a PEKM technikának, ami akadályozza a gyors, és nagyfelbontású képek rögzítését. A kép vagy gyorsan elkészül de torzított lesz, vagy jó minőségű, de nem pillanatszerű. Így a kép egyes pontjainak nem csak eltérő térbeli, de eltérő időbeli koordinátái is lesznek.

A disszertációmban ennek a problémának a megoldására irányuló munkámat írom le, és bemutatok három megoldást, melyeket kidolgoztam:

1. Újszerű, szilárd kontaktusú mikroelektródok használata mérőcsúcsként a hagyományos, folyadék kontaktusúak helyett.

2. A pásztázási mintázatok és algoritmusok optimalizálása.

3. A nagy sebességgel rögzített, de torzított képek dekonvolúciója.

Első megközelítésben megpróbáltam az indikátor elektród ellenállását csökkenteni. A hagyományos folyadék kontaktus helyett, vezető polimer alapú, szilárd belső kontaktus használatával a potenciometriás mérőcella ellenállása, és így időállandója csökkenthető. Vezető polimereket használtak már korábban, de nem célzottan magnézium ion-szelektív mikroelektródok ellenállásának csökkentésére.

A második módszer amit kidolgoztam a pásztázási mintázatok és algoritmusok optimalizálása. A legtöbb tanulmányozott rendszer meghatározott, egyszerű szimmetriával bír, melyre optimalizálható a pásztázás, a kisebb torzítás érdekében. Egy egyszerű, de gyakori szimmetriát, a körszimmetriát választottam, és kidolgoztam két optimalizált pásztázási mintázatot és hozzájuk tartozó algoritmust.

A harmadik technika amit alkalmaztam, a képfeldolgozás volt. A potenciometriás cella időbeli válaszát leíró függvény jól ismert. Néhány könnyen mérhető paraméter birtokában egy dekonvolúciós függvény megadható. Ennek segítségével az egyensúlyi potenciál megjósolható a kép minden egyes mintavételi pontjára, és a torzítás drasztikusan csökkenthető.

Ezen technikák hatékonyságát először modellrendszereken vizsgáltam, majd korróziós tanulmányokban mutattam be alkalmazhatóságukat. Több együttműködés során használtam a kidolgozott módszereket, és néhány eredményt ezek közül is bemutatok a disszertációmban.

Vizsgáltam továbbá az elektromos tér hatását a potenciometriás PEKM képalkotásra, mely sok vizsgált rendszerben jelen van. Bizonyos esetekben, ahol nagy potenciálkülönbség van a vizsgált rendszer különböző pontjai között, erős elektromos tér alakul ki. Ilyen például a galvanikus korrózió, mely során nagy potenciálkülönbség van a galvánpárok felületei között. Az elektromos potenciál mérőcsúcsnál jelentkező értéke befolyásolja a mért értéket. Megvizsgáltam ezen hatás nagyságát, és megpróbáltam elkülöníteni az elektromos tér hatását.

2. Módszerek

A disszertációmban bemutatott mérések nagyrészt nagy impedanciájú potenciál különbség mérések. Az impedanciaillesztést vagy a műszer biztosította, vagy egy külső, TL082 műveleti erősítő alapú feszültségkövető áramkör. Erre a terhelési hiba kiküszöbölése miatt volt szükség, mely a nagyon eltérő impedanciájú egységek illesztésekor lép fel. Ilyen hatás léphet fel például mikroelektródok potenciáljának mérése során.

Szinte az összes méréshez házi készítési PEKM egységet és saját készítású szoftvert használtam. Az összes bemutatott ion szelektív elektród saját készítésű volt. A következő indikátor elektródokat használtam:

- pH érzékeny antimon mikroelektród.
- pH érzékeny volfrám mikroelektród.
- Magnézium-ion szelektív mikropipetta.
- Kálium-ion szelektív mikropipetta.

Az indikátor elektród potenciálját mindig egy Ag/AgCl/(3 M) referencia félcellával szemben mértem. A dekonvolúciót, a diffúzió és PEKM szimulációkat FORTRAN nyelven írtam.

3. Results and Discussion

3.1. Using solid-contact microelectrodes as potentiometric SECM probes

Solid-contact electrodes have lower resistance, compared to their otherwise identical, liquid-contact counterparts. This is due to two reasons. The solid contact can be pushed down very close to the micropipette orifice, shortening the thickness of the highly resistive ion-selective membrane, and decreasing the overall electrode resistance. The other reason is that instead of the internal solution – which has high resistance –, a modified carbon fiber – which has low resistance – is used as the ion-to-electron transducer. If R is lower, RC is lower, and the potentiometric cell becomes faster.

I constructed two Mg^{2+}-ion selective electrodes. One used a liquid contact, and the other a solid contact. Besides this difference, they were prepared identically. Basic characterisation was performed for both. Response characteristics were investigated by measuring the electrode resistance R, and the τ_{95} response time. Calculated from the voltage divider measurements, electrode resistance was 4.8 GΩ and 0.56 GΩ for the liquid, and solid contact electrodes, respectively. Based on these values, the solid contact electrode was expected to produce less distorted images with the same scanning parameters.

To confirm it, a Mg^{2+} ion diffusion source model system was created, and the plane 100 µm above the pipette orifice was scanned with both electrodes. Fig. 1 shows the ISME images obtained using a liquid-contact (A), and a solid-contact (B), micropipette electrode. Both 2D ISME maps were recorded at the same scan rate.

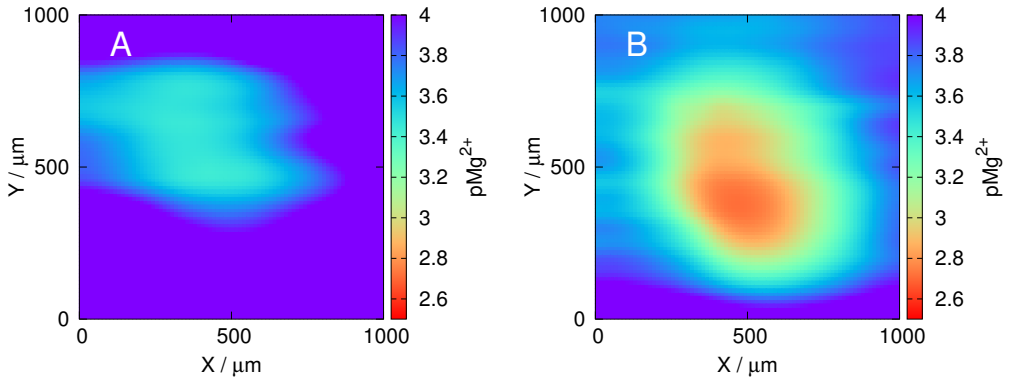

1. ábra. SECM images displaying the Mg^{2+} ion concentrations 100 µm above the tip of a centered pipette source. (A) liquid-contact, and (B) solid-contact. Scan rate: 12.5 µm/s.

An upside down glass micropipette holding the 0.1 M $MgCl_2$ agar solution was used in the measurements plotted in Figs. 1A and 1B. Visual inspection of the two images clearly shows significant image distortion in the X-direction with the liquid-contact ISME due its slower response as expected based on its higher resistance. It can also be observed in the image scanned with the solid-contact electrode, although to a much less extent. Another important feature to note in the images is the difference in the highest magnesium ion concentration observed with the two electrodes. With the solid-contact microelectrode it's about $10^{-2.5}$ M. On the other hand, with the conventional liquid-contact electrode, highest observed magnesium ion concentration is only about $10^{-3.4}$ M. One possible reason for this is that the cell equipped with the liquid-contact electrode cannot keep up with the changes of the magnesium ion concentration at the micropipette orifice.

One application that is included in my dissertation is the investigation of the galvanic corrosion of magnesium and its alloys. A solid contact magnesium ISME was used to map magnesium ion distribution above a corroding AZ63 magnesium-aluminium alloy. Vertical Mg^{2+} ion concentration distribution was determined at different instants in time of the corrosion process, with, and without coupling the Mg/Al and Fe samples. Using the Mg^{2+} concentration profiles, Mg^{2+} flow rate from the Mg piece was possible to estimate:

$$\Omega = 4DC_s a \tag{1}$$

where Ω is the amount of Mg^{2+} released from the disc shaped Mg/Al surface, D is the diffusion coefficient of Mg^{2+}, C_s is the surface concentration of Mg^{2+} (at the height $z = 0$ µm), a is the radius of the Mg/Al sample. As the only unknown variable in the equation above, Ω could be calculated.

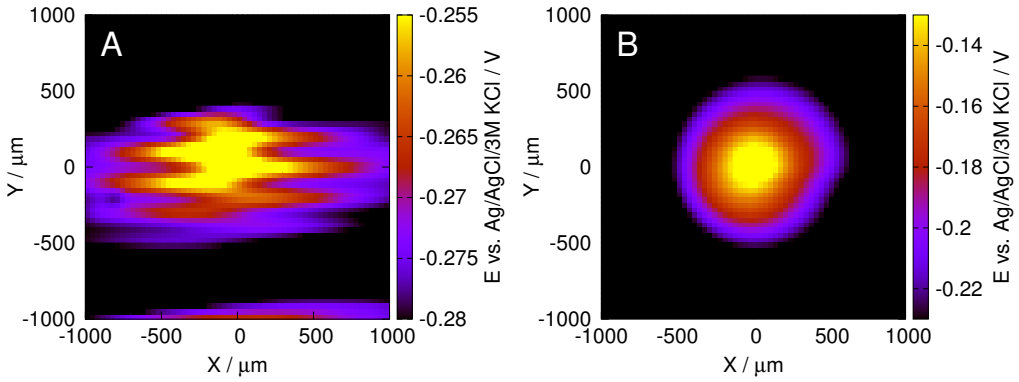

2. ábra. Experimental SECM scans 100 µm above the disc source with the (A) meander and the (B) arc scanning algorithms. Measuring electrode was a pH-sensitive antimony micro-electrode.

Corrosion current between the Mg/Al sample and the Fe sample was also measured directly. Using Faraday's law of electrolysis, corrosion current could be calculated, and it was in fairly good agreement with the SECM measurement.

3.2. Optimization of scanning algorithms

In the second and third approaches I exploit the properties of the potentiometric response function:

$$E_{cell}(t_e) = E_{cell}(\infty) + [E_{cell}(0) - E_{cell}(\infty)]e^{-t_e/RC} \tag{2}$$

where $E_{cell}(t)$ is the cell potential difference at time t_e, $E_{cell}(\infty)$ is the equilibrium cell potential difference, $E_{cell}(0)$ is the cell potential difference prior to the change. The more different $E_{cell}(0)$ and $E_{cell}(\infty)$ are, the more the difference between $E_{cell}(\infty)$ and $E_{cell}(t_e)$ will be. Distortion of an image can be measured as an average of the differences between $E_{cell}(\infty)$ and $E_{cell}(t_e)$ at each point. It can be lowered by carefully optimizing scanning patterns and algorithms, so that the probe passes through borders between regions of high and low concentrations as few times as possible.

The results (Figure 2) confirmed the presumption, that using the two new algorithms, images have less distortion, with higher similarity to the expected image.

3.3. Signal processing in potentiometric SECM

In the third approach, I use the inverse of the potentiometric response function (Eq. 2) as deconvolution function. Since the relationship between t_e, $E_{cell}(0)$, $E_{cell}(t_e)$

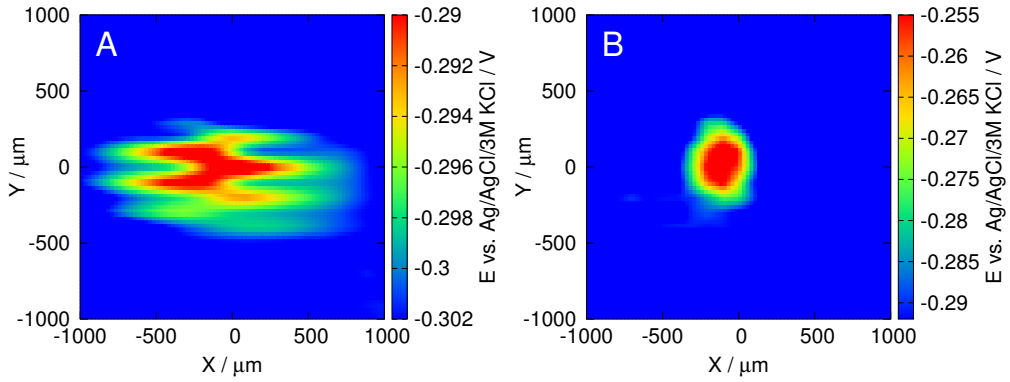

3. ábra. SECM pH image before (A) and after (B) deconvolution. Scan conducted with the antimony microelectrode. Note the different potential scales. Deconvolution restores not only the shape of the concentration profile, but the magnitude of the peak as well. The raster scan pattern was used with the meander algorithm starting in the bottom left corner of the image.

and $E_{cell}(\infty)$ is known, a prediction for the only unknown $E_{cell}(\infty)$ can be calculated.

2D SECM scan was performed above a circular graphite anode (Fig. 3A), with the meander scanning algorithm. Line blur distortion in the raw images is visible along the alternating scanlines used by the meander scanning algorithm. By deconvoluting the image, the expected potential map can be obtained (Fig. 3B).

Not only the circular shape of the target in the images is restored, but the peak value above the center of the target as well. Maximum value in the raw scans was around -300 mV, whereas in the deconvoluted image, it was about -260 mV, with a significant difference between the two.

I obtained similar results with ionophore based ion selective micropipettes, which can be found in my dissertation. I haven't included those results here, due to the compact format of this booklet.

As an example of the application of the technique, corroding carbon steel was imaged. As expected, the image was distorted, and without any processing evaluation proved to be difficult. The irregular shape of the target was recognisable after, but not before the deconvolution. The difference between the original and the processed image was quite large. Without any processing, pH would have been misestimated by about 1 pH unit. A different conclusion can be drawn based on the raw, and the deconvoluted image.

Another studied technique was blind deconvolution. This is the technique of deconvoluting measured data without the complete knowledge of the transfer function that describes the convolution. To explore this possibility, I deconvoluted a pH image using the deconvolution function with several different time-constant substitutions,

including the measured one.

The best result could be easily recognized just by visual inspection, and it was the one that was deconvoluted by the correct, measured time-constant. A more advanced method would be a statistical approach, where one would try to detect any correlation between the scanning algorithm – taking into account the scan direction – and the image, and choose the deconvoluted image with the least correlation.

3.4. The effect of electric field on potentiometric SECM images

During galvanic corrosion, ions are being released from the anode. The measured potential of an ion selective microelectrode is thought to depend only on the activity of the primary ion. However, an electric field is also formed as a result of the potential difference between the surfaces of the galvanic pair, which has a direct influence on the potential of the measuring microelectrode. The measured potential is the sum of these two contributions:

$$\Delta E = E_M - E_R + (\phi_M - \phi_R) \tag{3}$$

where ΔE is the measured potential difference, E_M and E_R is the potential of the measuring and the reference electrode, and ϕ_M and ϕ_R are the local potentials in the electric field at the measuring and reference electrodes, respectively.

There are multiple papers featuring contradictory results obtained by studying system where a strong electric field is present. These contradictory results can be explained by a contribution of the electric field that is formed during these experiments.

The ISME was maintained at a constant height from the metal surface, and its potential was recorded as a function of time, while the galvanic connection was established between the two metals (Fig. 4). Thus, the tip was first positioned 100 µm above the center of the AZ63 wire (red curve in Fig. 4), and for about 300 s the spontaneous corrosion of the alloy sample was recorded. Then, the galvanic connection was established, and a sharp increase in potential of about 70 mV could be observed. This change would correspond to a two orders of magnitude increase of Mg^{2+} activity in a very short period of time. When the galvanic connection was removed, a potential change of the same magnitude, though opposite direction could be observed. In order to discard the possibility that this rise could be still explained by an abrupt release of Mg^{2+} from the surface, the experiment was repeated while the tip was positioned 1000 µm above the target (blue curve in Fig. 4). A very similar sequence of potential changes could be observed, despite the big separation between the probe and the corroding sample. The only plausible explanation is that

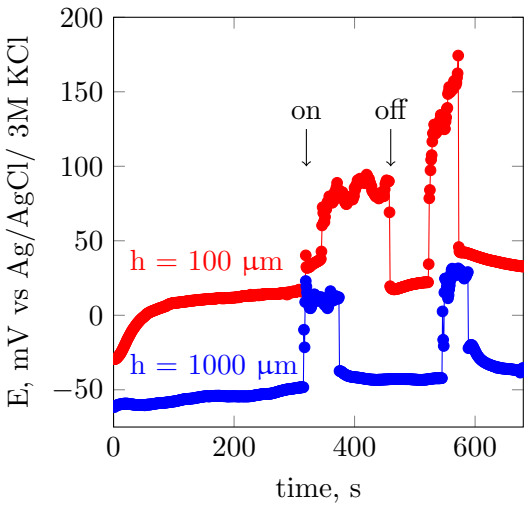

4. ábra. Stationary recordings above the center of the AZ63 target with the ISME placed at: red = 100 µm, blue = 1000 µm distance from the metal. On/off denote the moment when galvanic coupling was either established or ceased. Temporal resolution was 1 Hz.

the abrupt change in the recorded potential is due to the electric field developed between the two metals.

The effect of the electric field in certain potentiometric SECM experiments has been demonstrated experimentally, as suspected by certain researchers in corrosion science for some time. A strong electric field is formed around galvanic coupling of dissimilar metals, that causes significant over- or underestimations of the real primary ion activity. The reason for this feature is that the electric field has a direct influence on the measured potential at the ISME.

4. Conclusions

The present work has been devoted to improve potentiometric Scanning Electrochemical Microscopy. Scanning is relatively slow due to the long response time of the potentiometric measuring cell. Shortened scanning time is useful when the studied system is changing. When scanned too fast however, distortion is added to the image. I've successfully sped up the technique without compromising image quality. In another effort, I've managed to separate the effect of electric field from the Nernstian potential response of the ion selective microelectrode.

The main results are summarized in the thesis points:

1. I've successfully shortened response time of the potentiometric cell by using low resistance, solid-contact microelectrodes. I've compared them to conventio-

nal, liquid contact microelectrodes by basic characterization and model system study to prove the improved performance.

2. Taking adventage of the new solid-contact electrodes, I've studied the galvanic corrosion of magnesium and the AZ63 magnesium alloy by mapping the concentration of dissolving ions. I used the new solid contact ion selective microelectrodes as SECM probes. This allowed faster scan rates.

3. I've estimated the corrosion current based on the SECM measurements, and compared the result with that obtained with another, established method; the indirect measurement of corrosion current. After applying Faraday's Law of Electrolysis, the two results could be compared. They were very similar, suggesting the applicability of SECM in obtaining quantitative results.

4. I've designed new scanning patterns and algorithms, optimized to radially symmetric targets. I've proven that with these new patterns and algorithms, image distortion is lower compared to the conventional ones, by numerical simulations and experimental SECM scans.

5. I've shown that by using deconvolution, RC distortion can be significantly lowered in the potentiometric SECM images. To prove the validity of the technique, I've compared deconvoluted images to equilibrium images scanned at a rate which allowed to record equilibrium potentials.

6. I've used deconvolution to restore potentiometric SECM images about a corroding carbon steel sample. Evaluation of this data was possible, because scanning time *and* distortion was reduced at the same time.

7. I've shown the applicability of blind deconvolution. This method can be used on measurements where the convolution function cannot be determined.

8. I've proven that the electric field present in many studied systems – galvanically corroding ones in particular – affects the measured potential. The electric field has a direct influence on the measured potential, which is then a sum of this contribution and the Nernstian response associated with ion activity. This effect can cause serious errors in interpretations in the measurements. In this case, the error was almost four orders of magnitude. By taking this effect into account, a more accurate conclusion can be drawn.

5. Publications

5.1. Peer-reviewed publications related to the dissertation

1. Ricardo M. Souto, **András Kiss**, Javier Izquierdo, Lívia Nagy, István Bitter, Géza Nagy, Spatially-resolved imaging of concentration distributions on corroding magnesium-based materials exposed to aqueous environments by SECM, *Electrochemistry Communications 26 (2013): 25-28.*, IF.: 4.85, cited by: 31

2. **András Kiss**, Ricardo M. Souto, Géza Nagy, Investigation of Mg/Al alloy sacrificial anode corrosion with Scanning Electrochemical Microscopy, *Periodica Polytechnica Chemical Engineering 57, no. 1-2 (2013): 11-14.*, IF.: 0.30, cited by: 5

3. Javier Izquierdo, **András Kiss**, Juan José Santana, Lívia Nagy, István Bitter, Hugh S. Isaacs, Géza Nagy, Ricardo M. Souto, Development of Mg^{2+} ion-selective microelectrodes for potentiometric scanning electrochemical microscopy monitoring of galvanic corrosion processes, *Journal of The Electrochemical Society 160, no. 9 (2013): C451-C459.*, IF.: 3.27, cited by: 23

4. **András Kiss**, Géza Nagy, New SECM scanning algorithms for improved potentiometric imaging of circularly symmetric targets, *Electrochimica Acta 119 (2014): 169-174.*, IF.: 4.50, cited by: 8

5. **András Kiss**, Géza Nagy, Deconvolution of potentiometric SECM images recorded with high scan rate, *Electrochimica Acta 163 (2015): 303-309.*, IF.: 4.50, cited by: 7

6. **András Kiss**, Géza Nagy, Deconvolution in potentiometric SECM, *Electroanalysis 27, no. 3 (2015): 587-590.*, IF.: 2.14, cited by: 2

7. **András Kiss**, Dániel Filotás, Ricardo M Souto, Géza Nagy, The effect of electric field on potentiometric Scanning Electrochemical Microscopic imaging, *Electrochemistry Communications 77 (2017): 138-141.*, IF.: 4.569

5.2. Presentations and posters related to the dissertation

1. Investigation of Mg/Al alloy sacrificial anode corrosion with Scanning Electrochemical Microscopy, Poster, *Chemical Engineering Workshop '12, Veszprém, 2012.*

2. Investigation of galvanic corrosion of the Fe-Mg galvanic pair with Scanning Electrochemical Microscope, Poster, *Chemical Sensors Workshop '12, Pécs, 2012.*

3. Fabrication of a new, solid contact Mg^{2+} ion-selective electrode, and its application in Scanning Electrochemical Microscopic corrosion studies, Presenttion, *1st Doctoral Workshop on Natural Sciences, Pécs, 2012.*

4. A new, solid contact Mg^{2+} ion-selective electrode as measuring tip for Scanning Electrochemical Microscope in corrosion studies, Presentation, *János Szentágothai Memorial Conference and Student Competition, Pécs, 2012 October 29-30.*

5. New insights in the corrosion mechanism of magnesium by SECM, Presentation, *7th Workshop on Scanning Electrochemical Microscopy (SECM) and Related Techniques, Ein Gedi, Israel, February 17-21, 2013.*

6. High-speed potentiometric SECM imaging of radially symmetric targets, Presentation, *ESEAC Malmö, Sweden, 11-14 June 2013.*

7. Deconvolution of potentiometric SECM images recorded with high scanrate, Poster, *Mátrafüred Conference 2014 Június 13-16, Visegrád, Hungary.*

8. High-speed SECM imaging, Plenar presentation, *Analytica Conference 2016 May 10-13, München, Germany.*

5.3. Peer-reviewed publications unrelated to the dissertation

1. **András Kiss**, László Kiss, Barna Kovács, Géza Nagy, Air Gap Microcell for Scanning Electrochemical Microscopic Imaging of Carbon Dioxide Output. Model Calculation and Gas Phase SECM Measurements for Estimation of Carbon Dioxide Producing Activity of Microbial Sources, *Electroanalysis 23, no. 10 (2011): 2320-2326.*, IF.: 2.14, cited by: 3

2. Ricardo M. Souto, Javier Izquierdo, Juan José Santana, **András Kiss**, Lívia Nagy, Géza Nagy. Progress in scanning electrochemical microscopy by coupling potentiometric and amperometric measurement modes, *Current Microscopy Contributions to Advances in Science and Technology, Formatex Research Center, Badajoz (2012): 1407-1415*, cited by: 3

3. Lívia Nagy, Gergely Gyetvai, **András Kiss**, Ricardo Souto, Javier Izquierdo, Géza Nagy, Speciális célra szolgáló mikroelektródok kifejlesztése és alkalmazása, *Magyar Kémiai Folyóirat 119, 2-3. (2013): 104-109.*

4. Zsuzsanna Őri, **András Kiss**, Anton Alexandru Ciucu, Constantin Mihailciuc, Cristian Dragos Stefanescu, Lívia Nagy, Géza Nagy, Sensitivity enhancement of a „bananatrode" biosensor for dopamine based on SECM studies inside its reaction layer, *Sensors and Actuators B: Chemical 190 (2014): 149-156.*, IF.: 4.10, cited by: 4

5. Javier Izquierdo, Bibiana M Fernández-Pérez, Dániel Filotás, Zsuzsanna Őri, **András Kiss**, Romen T Martín-Gómez, Lívia Nagy, Géza Nagy, Ricardo M Souto, Imaging of Concentration Distributions and Hydrogen Evolution on Corroding Magnesium Exposed to Aqueous Environments Using Scanning Electrochemical Microscopy, *Electroanalysis 28, (2016): 2354-2366.*, IF.: 2.471, cited by: 2

6. A. El Jaouhari, Dániel Filotás, **András Kiss**, M. Laabd, E. A. Bazzaoui, Lívia Nagy, Géza Nagy, A. Albourine, J. I. Martins, R. Wang, SECM investigation of electrochemically synthesized polypyrrole from aqueous medium, *Journal of Applied Electrochemistry 46 (2016): 1199-1209.*, IF.: 2.223

5.4. Presentations and posters unrelated to the dissertation

1. CO_2 Partial Pressure Imaging in Gas Phase with Scanning Electrochemical Microscopy (SECM), Poster, *X. CECE Conference, Pécs, 2010.*

2. Selective Amperometric Determination Of Pyrocatechol and Phenol in Wines with Flow-Injection Analysis, Poster, *X. CECE Conference, Pécs, 2010.*

3. Four-Channel Enzyme Biosensor for Determination of Phenols in Wine, Poster, *X. CECE Conference, Pécs, 2010.*

4. Development of a CO_2 microcell, and its application as measuring tip in Scanning Electrochemical Microscope. Scanning in gas phase over biological samples, Presentation, *XXXIV. Szegedi Kémiai Előadói Napok, Szeged, 2011.*